第 44 卷　第 2 期
2024 年 2 月

$Na_{0.44}MnO_2$ 颗粒尺寸对其作为水系钠离子电池正极性能的影响

黄璧成　余灵辉　葛婧捷　徐梽川*
(南洋理工大学 材料科学与工程学院 新加坡 639798)

Tuning Particle Size of $Na_{0.44}MnO_2$ for Aqueous Na-Ion Battery Cathode

HUANG Bicheng, YU Linghui, GE Jingjie, XU Zhichuan*
(*School of Material Science and Engineering*, *Nanyang Technological University*, *Singapore* 639798, *Singapore*)

Abstract Aqueous sodium-ion battery is a complementary technique to lithium-ion battery because of its comparatively low cost, improved safety, and environmentally friendly electrolyte. However, the lower electrode capacity limits the application of this kind of batteries. $Na_{0.44}MnO_2$ is a high capacity cathode for Na-ion batteries. Its theoretical capacity is 121 mAh/g. In this article, we investigate the size effect of $Na_{0.44}MnO_2$ on cathode performance. The nanorods are prepared by heat treatment of a MnO_2 nanoflake precursor, of which the size is tuned by the ratio of CTAB and $KMnO_4$. The $Na_{0.44}MnO_2$ nanorods are then used as the active material of cathode for aqueous sodium-ion batteries. The nanorod cathode delivers 60 mAh/g in the initial cycle at 1 C and retains 55 mAh/g after 200 cycles, which is 37.5% higher than $Na_{0.44}MnO_2$ bulk cathode. This cathode gives a high capacity of 47 mAh/g after 200 cycles at a high rate of 5 C. The increased capacity is attributed to diminishing charge transfer resistance and improved Na-ion diffusivity caused by the higher specific surface area of the nanorod.

Keywords Na-ion battery, Cathode, Aqueous electrolyte, Size

摘要 水溶性钠离子电池是一种与锂离子电池相辅相成的技术，因其相对较低的成本、改善的安全性和环境友好的电解液而备受青睐。然而，较低的电极容量限制了这种电池的应用。$Na_{0.44}MnO_2$ 是一种用于钠离子电池的高容量阴极材料，其理论容量为 121 mAh/g。文章研究了 $Na_{0.44}MnO_2$ 的尺寸效应对阴极性能的影响。纳米棒通过热处理 MnO_2 纳米片前驱体制备而成，其尺寸通过 CTAB 和 $KMnO_4$ 的比例进行调控。然后，$Na_{0.44}MnO_2$ 纳米棒被用作水溶性钠离子电池的活性材料。纳米棒阴极在 1 C 的初始循环中提供了 60 mAh/g 的容量，并在经过 200 个循环后保持了 55 mAh/g，比 $Na_{0.44}MnO_2$ 块状阴极高出 37.5%。在高倍率的 5 C 下，该阴极在经过 200 个循环后仍能提供 47 mAh/g 的高容量。容量的增加归因于减小的电荷传递阻抗和纳米棒具有较高比表面积所带来的改善的钠离子扩散性能。

关键词 钠离子电池　正极　水系电解液　尺寸
中图分类号：O6　　**文献标识码**：A　　**doi**: 10.13922/j.cnki.cjvst.202307013

Introduction

Nowadays, commercial lithium-ion batteries (LIBs) are widely used for energy storage in our daily lives because of their high energy density and good cycling performance. However, safety and environmental issues, which arise from inflammable and toxic organic electrolytes, hinder their large-scale applications in some fields[1-4]. In contrast, aqueous sodium-ion batteries employ non-toxic aqueous electrolyte that is environmentally friendly and improves the safety of the batteries[5-8]. Besides, worldwide sodium reserves are much larger than lithium reserves, which could potentially reduce the cost of the sodium-ion batteries. Hence, high-performance aqueous sodium-ion batteries can be con-

---

收稿日期：2023−07−19

＊**联系人**：E-mail: xuzc@ntu.edu.sg

sidered a promising alternative in some specific large-scale applications.

Unfortunately, the energy density of the aqueous sodium-ion batteries is lower than that of LIBs. Both the narrow operational potential window and the limited capacity of the electrodes restrict the energy density of the batteries. Broadening the potential window would lead to either side reactions involving the aqueous electrolyte or irreversible phase transition of the electrodes. Therefore, exploring high-capacity electrodes at this limited potential window would be a more efficient in enhancing energy density of the batteries. In the search for high-capacity Na-ion cathodes, many types of active materials have been developed, such as oxides, polyanions, and Prussian blue analogs[9-18]. Among them, $Na_{0.44}MnO_2$ has drawn researchers' attention due to its large and stable S-shape and O-shape tunnels which facilitate Na ion insertion and extraction. The theoretical capacity of $Na_{0.44}MnO_2$ cathode is as high as 121 mAh/g. Besides, Mn-based oxides are low cost and environmentally benign materials[19-20]. Whitacre's work firstly demonstrated that a $Na_{0.44}MnO_2$ cathode could offer a long cycle life with a cycling capacity of 30-40 mAh/g at lower rates (0.2 C and 1.2 C) when charged and discharged from between −0.1 V and 0.7 V. This capacity would decrease to less than 20 mAh/g if the cathodes were cycled at a high rate of 18 C[21]. Low electrical conductivity or low Na-ion diffusivity are considered as possible causes of poor cycling stability and rate capability. Increasing the interfacial area between the electrolyte and the electrode by decreasing the size or dimension of the $Na_{0.44}MnO_2$ cathode would be available to improve the conductivity and the Na-ion diffusivity.

In this work, $Na_{0.44}MnO_2$ with different particle sizes are prepared to investigate the size effect on its cathode performance. Among these $Na_{0.44}MnO_2$, the nanorod one is found improved performance. By using α-MnO_2 nanoflakes as precursors, the $Na_{0.44}MnO_2$ nanorods were successfully prepared with a width of 200 nm. Such a size could enhance the electrical conductivity and the Na-ion diffusivity of the cathode. The as-prepared cathode shows a higher cycling capacity and lower polarization at a low rate of 1 C and a high rate of 5 C. The initial discharging capacity of $Na_{0.44}MnO_2$ nanorods cathode reaches 60 mAh/g at 1 C, with 55 mAh/g retained after 200 cycles. A high capacity of 47 mAh/g is delivered after 200 cycles at a high rate of 5 C. The high stability of thin $Na_{0.44}MnO_2$ nanorods is due to the stable morphology and crystal structure after long cycles.

1 Experimental

Synthesis of $Na_{0.44}MnO_2$ nanorods. $KMnO_4$ solution (0.01 mol/L) was heated at 100℃. Cetrimonium bromide (CTAB) solution (0.05 mol/L) was heated at 140℃. 100 mL of $KMnO_4$ solution was injected into 100 mL of CTAB solution. The color of the obtained solution gradually turned from purple to brown. 500 mL of acetone was added to the solution and brown precipitates were obtained. The precipitates were washed with deionized water by centrifugation and dried at 80℃ for 24 h. The dried powder was added to 30 mL aqueous $NaBH_4$ solution. The mixture was kept stirring at room temperature for 24 h. The obtained power was washed with deionized water by filtration and dried at 80℃ for 24 h. The dried powder was mixed and ground with $NaHCO_3$ in a mass ratio of 2∶1, and then heated in air at 500℃ for 5 h. After cooling down, the obtained powered was ground again and then heated at 900℃ in air for 12 h.

Synthesis of $Na_{0.44}MnO_2$ microrods. The synthesis procedure was the same as that for $Na_{0.44}MnO_2$ nanorods, except 0.1 mol/L $KMnO_4$ solution was used, instead of 0.01 mol/L.

Synthesis of $Na_{0.44}MnO_2$ bulk. Mn_2O_3 and $NaHCO_3$ were mixed and ground with 10% excess of Na in stoichiometry with the molar ratio of manganese atoms to sodium atoms as 1∶0.484. The mixture was heated in air at 500℃ for 5 h. After cooling down, the obtained powered was ground again and then heated at 900℃ in air for 12 h.

Material Characterizations. X-ray diffraction (XRD) patterns were collected on a Panalytical XPert

Pro X-ray diffractometer with Cu Kα radiation. Field emission scanning electron microscopy (FESEM) analysis was carried out on ZEISS Supra 55. High-resolution transmission electron microscopy (HRTEM) analysis was carried out using a JEOL 2100F at 200 kV. N_2 (77 K) adsorption test was conducted on an ASAP Tristar Ⅱ 3020. Brunauer−Emmett−Teller (BET) was used for the surface area determination. Inductively coupled plasma optical emission spectrometer (ICP-OES) test was conducted on a PerkinElmer@Optima 8300.

Electrochemical Measurements. Three-electrode system was used for the evaluation of the $Na_{0.44}MnO_2$. The working electrode was prepared by mixing $Na_{0.44}MnO_2$, single-walled carbon nanotube (SWCNT), and polytetrafluoroethylene (PTFE) at 8 : 1 : 1, followed by pressing the mixture on a 4 cm^2 Ni foam using a hydraulic press machine with a pressure of 10 MPa. The active mass loading was about 30 mg. A Pt foil was employed as a counter electrode and an Ag/AgCl (saturated NaCl) electrode was employed as a reference electrode. The electrolyte was 1 mol/L Na_2SO_4 in deionized water. Cyclic voltammetry (CV) measurement was conducted in a voltage range of −0.2 V to 0.8 V vs. Ag/AgCl at a scan rate of 0.1 mV/s. For galvanostatic charge-discharge (GCD) tests, the voltage window was controlled between −0.1 V and 0.7 V. 1 C corresponds to 121 mA/g in this work. Electrochemical impedance spectroscopy (EIS) was tested in the frequency range of 10 mHz to 100 kHz, and the perturbation amplitude is 5 mV. CV, GCD, and EIS were all measured on a Biological potentiostat electrochemical station.

2 Result and discussion

XRD was used to determine the structure of the prepared materials (Fig. 1(a)). All the diffraction peaks of the three materials can be assigned to the orthorhombic $Na_{0.44}MnO_2$ phase (Fig. 1(b)) [23]. The diffraction peaks are sharp and intense, which indicates the high crystallinity of the materials. HRTEM analysis shows interplanar spacing of 0.26 nm (Fig. 1(c)) and 0.45 nm (Fig. 1(d)) for $Na_{0.44}MnO_2$ nanorods and microrods, respectively. They correspond to (3 5 0) and (2 0 0) crystal planes of orthorhombic $Na_{0.44}MnO_2$, respectively. For $Na_{0.44}MnO_2$ bulk (Fig. 1(f)), interplanar spacings of 0.28 nm and 0.45 nm were determined, corresponding to (0 0 1), and (2 0 0) crystal planes, respectively. The ratios of Na/Mn in the three prepared materials were examined by ICP-OES (Table 1). They are all very close to 0.44. These demonstrate all the three prepared materials are $Na_{0.44}MnO_2$ with an orthorhombic structure.

The morphology and dimensions of the samples can be observed from SEM images displayed in Fig. 1(g), (h), and (i). $Na_{0.44}MnO_2$ bulk show varying dimensions with a wide size distribution. The bulk have lengths of 3−10 μm and widths of 0.5−1 μm. $Na_{0.44}MnO_2$ microrods have a smaller dimension than $Na_{0.44}MnO_2$ bulk, with a narrow size distribution and regular shapes. Its widths are smaller than 0.5 μm. A uniform rod shape can be observed in images of $Na_{0.44}MnO_2$ nanorods with widths of about 200 nm. The lengths of the nanorods range from 2 to 10 μm. The difference in morphology between the three samples may be caused by the using of CTAB as a surfactant. $Na_{0.44}MnO_2$ nanorods are prepared by using the largest CTAB/$KMnO_4$ ratio, and its widths are the smallest. $Na_{0.44}MnO_2$ microrods are prepared by using the smaller CTAB/$KMnO_4$ ratio, and its widths are larger than $Na_{0.44}MnO_2$ nanorods. CTAB is not needed when preparing $Na_{0.44}MnO_2$ bulk. The precursor of $Na_{0.44}MnO_2$ bulk, Mn_2O_3, has a wide size distribution and irregular shapes, leading to the inhomogeneous product after the solid-state reaction.

N_2 adsorption/desorption isotherms of the prepared materials are shown in Fig.1(c). All the samples display III-type isotherm curves with no hysteresis loop, indicating the materials are non-porous. The BET surface areas and average particle sizes based on this test are listed in Table 1. $Na_{0.44}MnO_2$ nanorods show the highest BET surface area of 4.1 m^2/g and the lowest average particle size of 1.45 μm, while $Na_{0.44}MnO_2$ bulk have the lowest BET surface area of 0.9 m^2/g and largest average particle size of 6.64 μm. The BET surface area of $Na_{0.44}MnO_2$ microrods is 2.7 m^2/g, and its

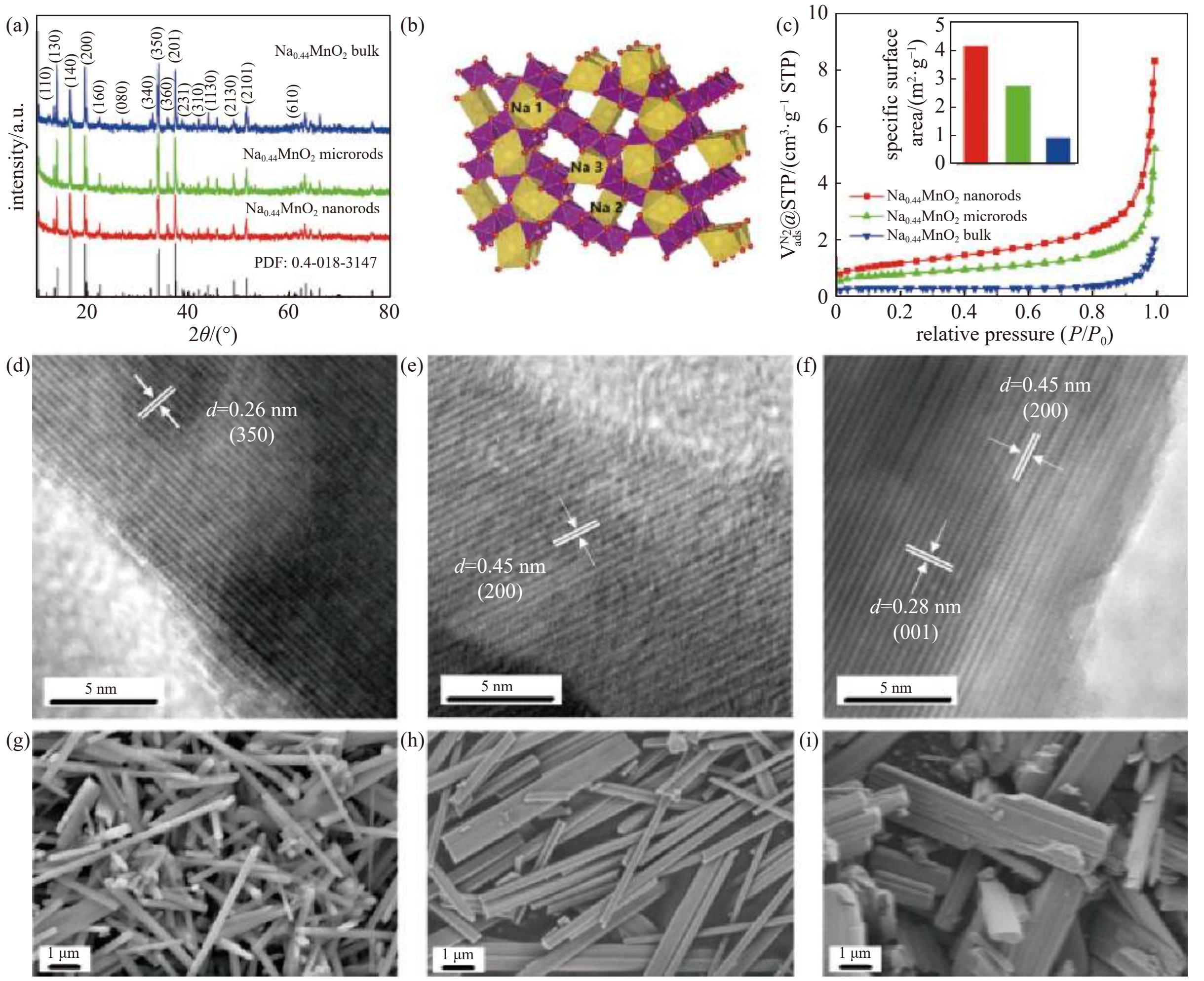

图1 材料表征。(a)三个 $Na_{0.44}MnO_2$ 样品的 XRD 粉末衍射图,(b) $Na_{0.44}MnO_2$ 晶体结构示意图,(c)三个样品的氮气吸附脱附曲线,插图为比表面积比较示意图,(d)(e)和(f)三个样品的高分辨投射电镜照片,(g)(h)和(i)三个样品的扫描电镜照片

Fig. 1 Materials characterizations. (a) XRD patterns of the three samples. (b) Crystal structure of $Na_{0.44}MnO_2$. (c) N_2 adsorption/desorption isotherms curves of the three samples, inset is the specific surface areas of the samples. HRTEM images of (d) $Na_{0.44}MnO_2$ nanorods (e) $Na_{0.44}MnO_2$ microrods, and (f) $Na_{0.44}MnO_2$ bulk; the scales are 5 nm. SEM images of (g) $Na_{0.44}MnO_2$ nanorods, (h) $Na_{0.44}MnO_2$ microrods, and (i) $Na_{0.44}MnO_2$ bulk, Mag= 10 kx, the scales are all 1 μm

Tab. 1 Na/Mn ratios, specific surface areas and particle sizes of the samples

	Na/Mn atom ratio	BET surface area /(m^2/g)	Average particle size /nm
$Na_{0.44}MnO_2$ nanorods	0.442	4.1426	1448.3825
$Na_{0.44}MnO_2$ microrods	0.439	2.7244	2202.2848
$Na_{0.44}MnO_2$ bulk	0.440	0.9038	6638.9706

average particle size is 2.20 μm. The trend that the three materials show in the isotherms is consistent with the SEM images.

Fig. 2(a) shows the typical CV curves (6th CV cycle) of the three materials. Five anodic peaks can be observed for all the three materials, i.e., peaks A, B, C, D, and E. Peak A corresponds to the extraction of Na in the Na3 site in the S-shaped tunnel (Fig. 1(b)). [24-26] Peaks B, D, and E are related to the 3-step Na extraction in the Na2 site in the S-shaped tunnel. Peak C is due to the extraction of Na in O-shaped tunnel (Na1 site). Multiple cathodic peaks are also observed, i.e., peaks A’ (A’^{,1} and A’^{,2}), B’, C’, D’, and E’, corresponding to A, B, C, D, and E, respectively. There are two cathodic peaks (A’^{,1} and A’^{,2}) corresponding to the anodic peak A, indicating the insertion/extraction of Na in the Na3 site is 2-step processes. The differences be-

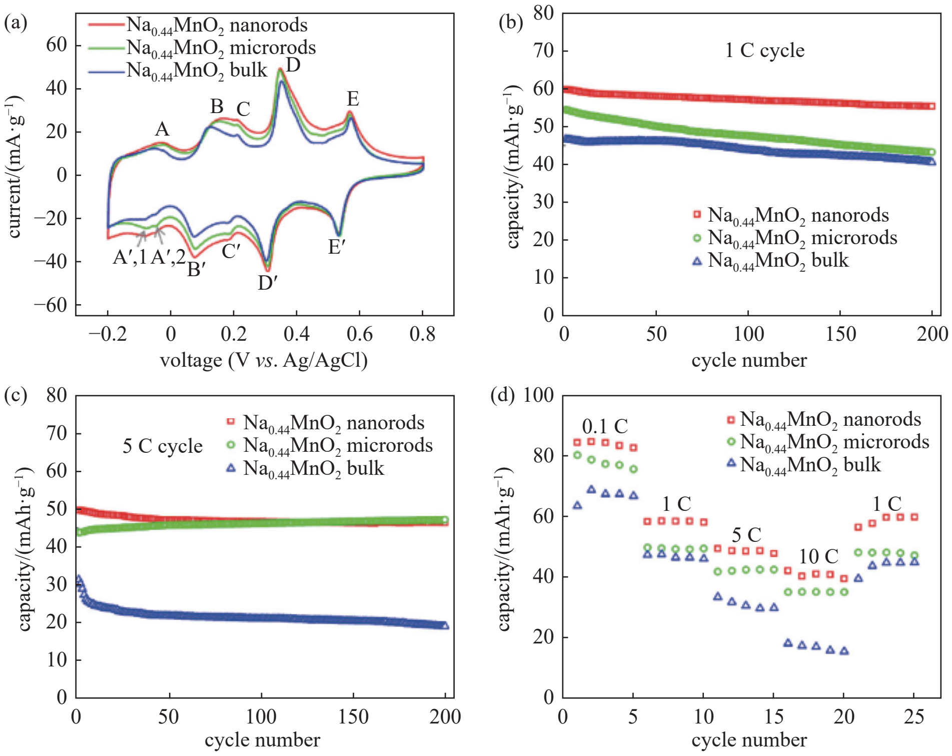

图2　电化学表征。(a)三个 $Na_{0.44}MnO_2$ 样品的稳定态循环伏安曲线(第 6 圈),(b)和(c)三个样品在 1C 和 5C 倍率下的循环性能,(d)三个样品的倍率性能

Fig. 2　Electrochemical characterizations. (a) The 6th CV curves of $Na_{0.44}MnO_2$ nanorods, $Na_{0.44}MnO_2$ microrods, and $Na_{0.44}MnO_2$ bulk. The profiles start to overlap since the 6th cycle. Cycling performances of $Na_{0.44}MnO_2$ nanorods cathode, $Na_{0.44}MnO_2$ microrods cathode, and $Na_{0.44}MnO_2$ bulk cathode (b) at 1 C, (c) at 5 C. (d) Rate performance of $Na_{0.44}MnO_2$ nanorods cathode, $Na_{0.44}MnO_2$ microrods cathode, and $Na_{0.44}MnO_2$ bulk cathode

tween the cathodic (2 peaks) and anodic (1 peak) processes for Na insertion/extraction in the Na3 site could be due to different kinetics during Na insertion/extraction. Only one anodic peak A observed is possibly because of the overlapping of the 2-step process.

Cycle performances of the three cathodes can be observed in Fig. 2(b) and (c). The corresponding galvanostatic charge/discharge (GCD) results of the three cathodes can be seen in Fig. 3. It is observed in GCD results that $Na_{0.44}MnO_2$ bulk cathode shows much higher polarization than the other 2 cathodes, especially at 5 C cycle. It should be attributed to the size differences of the materials. $Na_{0.44}MnO_2$ bulk has the largest particle size and the smallest BET surface area which could lead to the poorest conductivity and highest polarization among the three materials. Moreover, the initial discharging capacity of $Na_{0.44}MnO_2$ nanorods cathode is 60 mAh/g, and 55 mAh/g is retained after 200 cycles. $Na_{0.44}MnO_2$ microrods cathode delivers a capacity of 55 mAh/g in the 1st cycle and maintains 44 mAh/g in the 200th cycle. In contrast, the $Na_{0.44}MnO_2$ bulk cathode can only deliver a 46 mAh/g capacity in the first cycle, which decreases to 40 mAh/g after 200 cycles. The $Na_{0.44}MnO_2$ nanorods cathode exhibits a 37.5% higher capacity than $Na_{0.44}MnO_2$ bulk cathode due to the size difference of the active material. The polarization of $Na_{0.44}MnO_2$ bulk cathode increases severely at 5 C, while the polarization of $Na_{0.44}MnO_2$ nanorods cathode keeps stable in the first 50 cycles. The discharging capacity of $Na0_{.44}MnO_2$ nanorods cathode reaches 53 mAh/g at 5 C in the first cycle and maintains 47 mAh/g after 200 cycles. $Na_{0.44}MnO_2$ microrods cathode delivers a 44 mAh/g in the 1st cycle, while its capacity gradually increases with cycling and attains 47 mAh/g in the 200th cycle. This cycling capacity is the same as the $Na_{0.44}MnO_2$ nanorods cathode in the 200th cycle. In contrast,

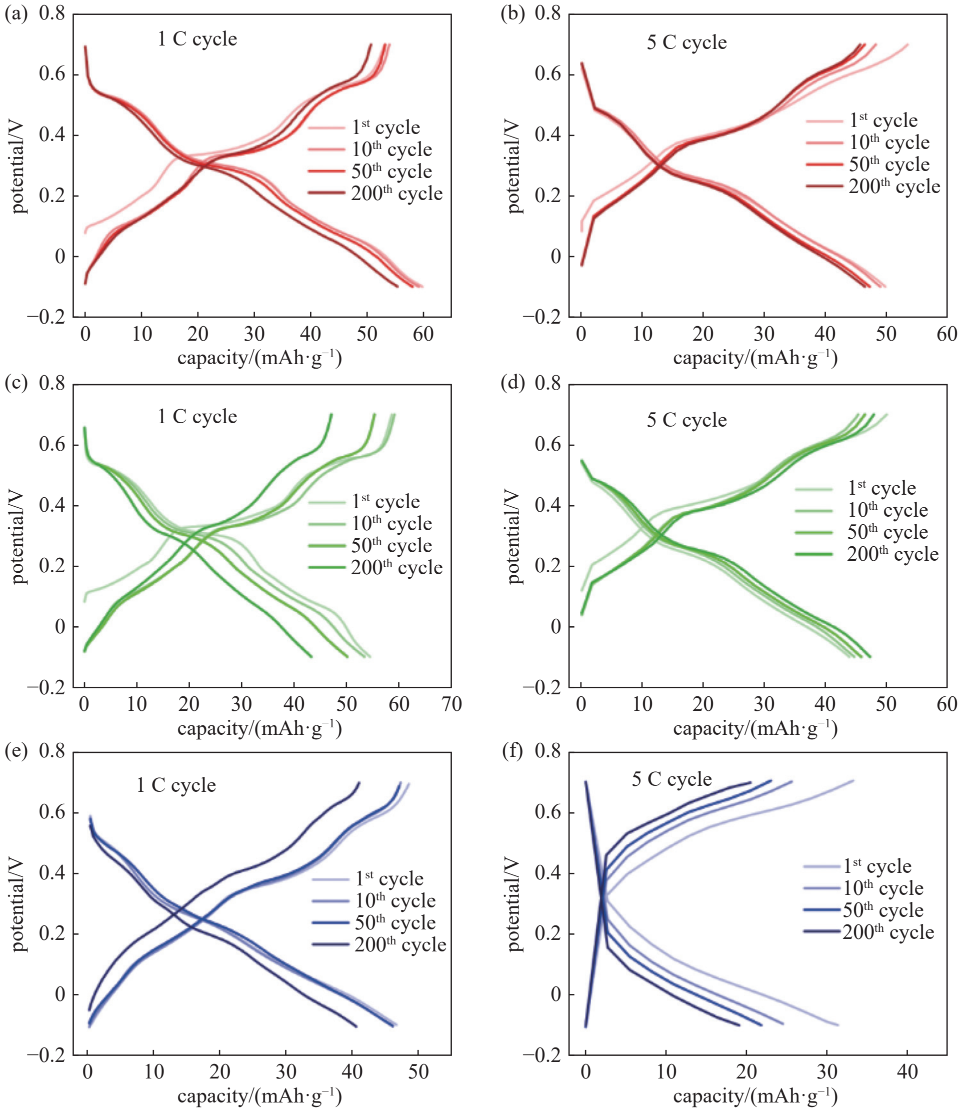

图3 充放电性能表征。(a)和(b)$Na_{0.44}MnO_2$ 纳米棒在 1C 和 5C 倍率下第 1、10、50、200 圈的充放电曲线,(c)和(d) $Na_{0.44}MnO_2$ 微米棒在 1 C 和 5 C 倍率下第 1、10、50、200 圈的充放电曲线,(a)和(b) $Na_{0.44}MnO_2$ 大颗粒在 1 C 和 5 C 倍率下第 1、10、50、200 圈的充放电曲线

Fig. 3 Charge/discharge properties. Galvanostatic charge/discharge curves in 1st , 10th , 50th , and 200th cycles of (a) $Na_{0.44}MnO_2$ nanorods cathode at 1 C, (b) $Na_{0.44}MnO_2$ nanorods cathode at 5 C, (c) $Na_{0.44}MnO_2$ microrods cathode at 1 C, (d) $Na_{0.44}MnO_2$ microrods cathode at 5 C, (e) $Na_{0.44}MnO_2$ bulk cathode at 1 C, and (f) $Na_{0.44}MnO_2$ bulk cathode at 5 C

$Na_{0.44}MnO_2$ bulk cathode can only deliver 32 mAh/g in the initial cycle when discharging, and this drops to 19 mAh/g after 200 cycles. The cycling capacity of $Na_{0.44}MnO_2$ nanorods at 5 C is 147 % higher than that of $Na_{0.44}MnO_2$ bulk cathode. The $Na_{0.44}MnO_2$ nanorods have the largest specific surface area and the smallest average particle size, which is good for the contact between the active material and the electrolyte. Hence, this cathode delivers the highest cycling capacity at 1 C and at 5 C.

The $Na_{0.44}MnO_2$ nanorods cathode exhibits correspondingly higher capacities in the rate test (Fig. 2(d)). The nanorod cathode delivers a very high capacity of 84 mAh/g at 0.1 C in the second cycle, 58 mAh/g at 1 C, 49 mAh/g at 5 C, 41 mAh/g at 10 C, respectively. It recovers to 56 mAh/g in the second cycle back at 1 C. All these capacities are the highest among the three cathodes. $Na_{0.44}MnO_2$ microrods cathode shows lower capacities than $Na_{0.44}MnO_2$ nanorods cathode and higher capacities than $Na_{0.44}MnO_2$ bulk cathode at each rate.

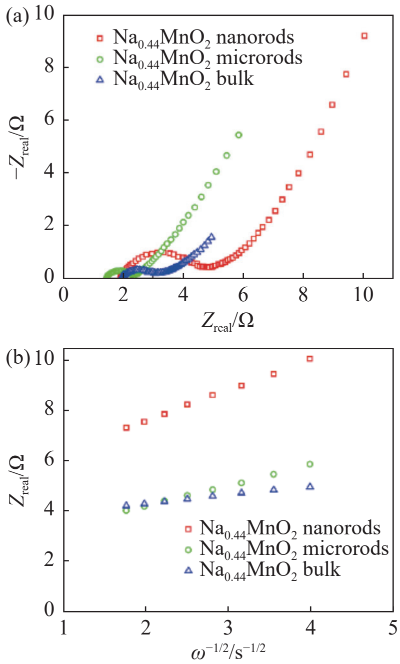

图4 电化学交流阻抗研究。(a)三个样品的电化学交流阻抗谱,(b)三个样品的 Z_{real} 和 $\omega^{-1/2}$ 的关系图

Fig. 4 Electrochemical impedance spectroscopy (EIS) study. (a) EIS of $Na_{0.44}MnO_2$ nanorods cathode, $Na_{0.44}MnO_2$ microrods cathode, and $Na_{0.44}MnO_2$ bulk cathode, (b) relationship between Z_{real} and $\omega^{-1/2}$ at low frequency of $Na_{0.44}MnO_2$ nanorods cathode, $Na_{0.44}MnO_2$ microrods cathode, and $Na_{0.44}MnO_2$ bulk cathode

Tab. 2 Ohmic resistance, charge transfer resistance, and diffusivity of Na ion of the cathodes

	$Na_{0.44}MnO_2$ nanorods	$Na_{0.44}MnO_2$ microrods	$Na_{0.44}MnO_2$ bulk
R_s / Ω	1.9	1.5	2.0
R_{ct} / Ω	3.0	0.9	1.2
D_{Na} / 10^{-14} cm^2s^{-1}	4.2	2.7	1.3

Meanwhile, the bulk cathode can only deliver 63, 47, 33, and 18 mAh/g at 0.1, 1, 5, and 10 C, respectively. It can only recover to just 39 mAh/g when the rate is back to 1 C. All these capacities are the lowest among the cathodes. The excellent rate performance of $Na_{0.44}MnO_2$ nanorods cathode implies wide applications at different rates.

To reveal the cause of the higher cycling capacity and the higher rate capacity of $Na_{0.44}MnO_2$ nanorods cathode, EIS of the cathodes has been conducted. Fig. 4 shows the Nyquist plots of three pristine cathodes. All the Nyquist plots display a semicircle at medium frequency followed by a slope at low frequency. The value that the semicircle begins corresponds to R_s (ohmic resistance of the electrode and electrolyte). The diameter of the half-circle corresponds to R_{ct} (charge transfer resistance). The slope depends on the diffusivity of ions that are conducted in the electrode. The $Na_{0.44}MnO_2$ bulk cathode shows a R_s and R_{ct} values of 2.0 and 1.2 Ω, respectively. The $Na_{0.44}MnO_2$ nanorods cathode shows a R_s of 1.9 and a R_{ct} and 3.0 Ω, respectively. The $Na_{0.44}MnO_2$ microrods cathode shows a R_s of 1.5 and a R_{ct} and 0.9 Ω, respectively. The three cathodes have the close ohmic resistances. For R_{ct}, The $Na_{0.44}MnO_2$ nanorods cathode owns the highest R_{ct} among the three cathodes, while the $Na_{0.44}MnO_2$ microrods cathode owns lowest R_{ct}.

The diffusivity of Na ion (D_{Na}) on the cathodes can be calculated to check the kinetics of the cathodes (Table 2). The equation calculating D_{Na} is shown as following: $D_{Na}=R^2T^2/2A^2n^4F^4C^2\sigma^2$, where R is gas constant, T is the testing temperature, A is the surface area of the cathode, n is the number of transferred electrons, F is Faraday constant, C is the concentration of the Na ion in the electrode, σ is Warburg coefficient[26]. By plotting Z_{real} and $\omega^{-1/2}$ at low frequency, σ can be obtained by calculating the slope of the fitting line. D_{Na} of $Na_{0.44}MnO_2$ nanorods cathode is calculated to be 4.2×10^{-14} cm^2s^{-1}. D_{Na} of $Na_{0.44}MnO_2$ microrods cathode is calculated to be 2.7×10^{-14} cm^2s^{-1} which is smaller than that of $Na_{0.44}MnO_2$ nanorods cathode. The $Na_{0.44}MnO_2$ bulk

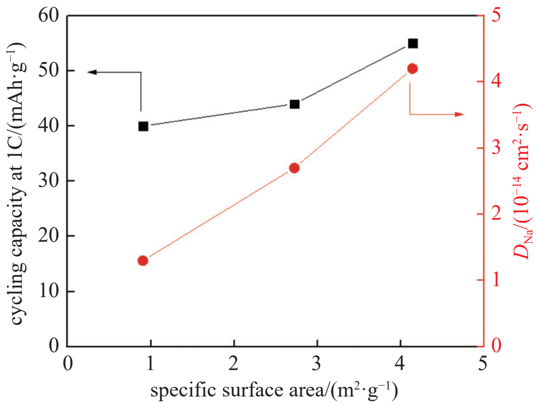

图5 循环性能、钠离子扩散率和材料比表面积的关系

Fig. 5 Relationship between cycling capacity, D_{Na}, and specific surface area cathode has the smallest D_{Na} of 1.3×10^{-14} cm^2s^{-1}. The largest D_{Na} of $Na_{0.44}MnO_2$ nanorods cathode demonstrates that the nanorods structure, with the highest BET surface area and the smallest particle size, can facilitate the Na ion transfer in the active materials during electrochemical reactions. This high Na ion can diffusivity contributes to the high capacity of this cathode. The relationship between cycling capacity, D_{Na}, and specific surface area is displayed in Fig. 5. It can be observed that the larger specific surface area corresponds to the higher D_{Na} and leads to the larger cycling capacity at 1 C. The similar trends of the two profiles in this figure reveal the potential influence of D_{Na} on the cycling capacity. It can be deduced that if the BET surface area of $Na_{0.44}MnO_2$ turns larger, its D_{Na} can be higher, and the cycling capacity of the cathode can be further enhanced.

The crystal information of the electrodes before and after the cycling test can be studied by XRD and HRTEM. XRD patterns of the samples and the corresponding cathodes before and after the cycling test are illustrated in Fig. 6(a), (c), and (e). No difference is

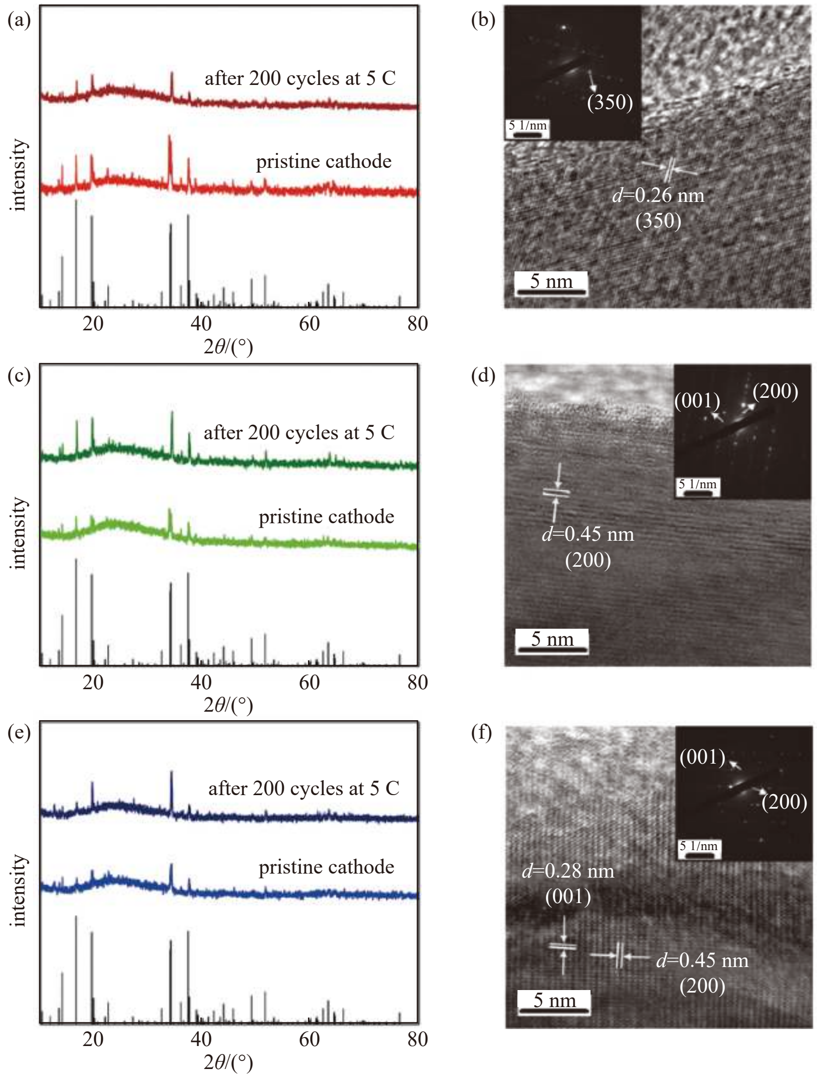

图6 充放电后电极的表征。(a)(c)和(e)三个样品在 5 C 倍率下充放电 200 圈后的 XRD 粉末衍射图，(b)(d)和(f)三个样品在 5 C 倍率下充放电 200 圈后的高分辨透射电镜照片以及相应的晶体选区电子衍射图

Fig. 6 Characterizations of electrodes after charge/discharge operation. XRD patterns of the cathodes before and after 200 cycles at 5 C cycling tests and the corresponding active materials, (a) $Na_{0.44}MnO_2$ nanorods, (c) $Na_{0.44}MnO_2$ microrods, and (e) $Na_{0.44}MnO_2$ bulk; HRTEM images of cathodes after 200 cycles at 5 C, (b) $Na_{0.44}MnO_2$ nanorods cathode, (d) $Na_{0.44}MnO_2$ microrods cathode, and (f) $Na_{0.44}MnO_2$ bulk cathode, inset images are SAED patterns of corresponding cathodes shown in peak positions between the patterns of the cathodes before and after the cycling tests, respectively. It means no new phase could be observed in the XRD patterns. The crystal lattices of the three cathodes after 5 C cycling are found in HRTEM images, Fig. 6(b), (d), and (f), respectively. The SAED patterns can confirm the existence of the crystals. The interplanar spacing of 0.28 nm and 0.45 nm can be correlated to (0 0 1) and (2 0 0) crystal plane, while the interplanar spacing of 0.26 nm can be correlated to (3 5 0) crystal plane. These parameters are the same as those of the active materials. The single crystal morphology and the maintained crystal interplanar spacings demonstrate that after 200 cycles at a high rate of 5 C, these three cathodes keep the lattices, and no phase transition happens after the cycling tests.

3 Conclusion

In summary, $Na_{0.44}MnO_2$ with different sizes have been prepared by reducing $KMnO_4$ in hot water followed by heat treatment with $NaHCO_3$. They are used in cathodes for aqueous Na-ion batteries. The nanorods with a width of ~ 200 nm gives the best cycling capacity and rate capacity. The initial discharging capacity of $Na_{0.44}MnO_2$ nanorods cathode attains 60 mAh/g at 1 C and it can remain 55 mAh/g after 200 cycles which is 37.5% higher than $Na_{0.44}MnO_2$ bulk cathode. At 5 C, the discharging capacity of $Na_{0.44}MnO_2$ nanorods cathode reaches 53 mAh/g in the first cycle and maintains 47 mAh/g after 200 cycles which is 147% higher than that of $Na_{0.44}MnO_2$ bulk cathode. Besides, the original orthorhombic $Na_{0.44}MnO_2$ phase of the $Na_{0.44}MnO_2$ nanorods maintains well after a high-rate cycling test at 5 C. This study demonstrates that the size of $Na_{0.44}MnO_2$ matters in the cathode performance. It indicates that reducing the size of active materials can be a promising way to explore high-capacity cathodes for aqueous Na-ion batteries.

Acknowledgements

This research was supported by the National Research Foundation, Prime Minister's Office, Singapore, under its Campus for Research Excellence and Technological Enterprise (CREATE) program. The authors thank the Facility for Analysis, Characterization, Testing and Simulation (FACTS) at Nanyang Technological University for materials characterizations.

参 考 文 献

[1] Nitta N, Wu F, Lee J T, et al. Li-ion battery materials: present and future[J]. Materials Today, 2015, 18(5): 252−264

[2] Etacheri V, Marom R, Elazari R, et al. Challenges in the development of advanced Li-ion batteries: a review[J]. Energy & Environmental Science, 2011, 4(9): 3243−3262

[3] Zeng X, Li J, Singh N. Recycling of spent lithium-ion battery: a critical review[J]. Critical Reviews in Environmental ence & Technology, 2014, 44(10): 1129−1165

[4] Chu S, Majumdar A. Opportunities and challenges for a sustainable energy future[J]. Nature, 2012, 488(7411): 294−303

[5] Sun Y, Guo S, Zhou H. Exploration of advanced electrode materials for rechargeable sodium-ion batteries[J]. Advanced Energy Materials, 2019, 9(23): 1800212.1−1800212.18

[6] Bin D, Wang F, Tamirat A G, et al. Progress in aqueous rechargeable sodium-ion batteries[J]. Advanced energy materials, 2018, 8(17): 1703008.1−1703008.31

[7] Che H, Chen S, Xie Y, et al. Electrolyte design strategies and research progress for room-temperature sodium-ion batteries[J]. Energy & Environmental ence, 2017, 10(5): 1075−1101

[8] Suo L, Borodin O, Wang Y, et al. "Water-in-Salt" electrolyte makes aqueous sodium-ion battery safe, green, and long-lasting[J]. Advanced Energy Materials, 2017, 7(21): 1701189.1−1701189.13

[9] Jung Y, Hong S, Kim D. Electrochemical sodium ion intercalation properties of $Na_{2.7}Ru_4O_9$ in nonaqueous and aqueous electrolytes[J]. Journal of the Electrochemical Society, 2013, 160(6): A897−A900

[10] Wang Y, Mu L, Liu J, et al. A novel high capacity positive electrode material with tunnel-type structure for aqueous sodium-ion batteries[J]. Advanced Energy Materials, 2015, 5(22): 1501005.1−1501005.8

[11] Zhang X, Hou Z, Li X, et al. Na-birnessite with high capacity and long cycle life for rechargeable aqueous sodium-ion battery cathode electrodes[J]. Journal of Materials Chemistry A, 2016, 4(3): 856−860

［12］ Zhang Y, Yuan C, Ye K, et al. An aqueous capacitor battery hybrid device based on Na-ion insertion-deinsertion in λ-MnO2 positive electrode[J]. Electrochimica Acta, 2014, 148: 237−243

［13］ Song W, Ji X, Zhu Y, et al. Aqueous sodium-ion battery using a $Na_3V_2(PO_4)_3$ electrode[J]. Chem Electro Chem, 2014, 1(5): 871−876

［14］ Fernandez-Ropero A J, Saurel D, Acebedo B, et al. Electrochemical characterization of $NaFePO_4$ as positive electrode in aqueous sodium-ion batteries[J]. Journal of Power Sources, 2015, 291(30): 40−45

［15］ Zhang Y, Ye K, Cheng K, et al. Three-dimensional lamination-like P2-$Na_{2/3}Ni_{1/3}Mn_{2/3}O_2$ assembled with two-dimensional ultrathin nanosheets as the cathode material of an aqueous capacitor battery[J]. Electrochimica Acta, 2014, 148: 195−202

［16］ Qing Z, Yong L, Jun C. Advanced organic electrode materials for rechargeable sodium-ion batteries[J]. Advanced Energy Materials, 2017, 7(8): 1601792.1−1601792.22

［17］ Wu X, Sun M, Shen Y, et al. Energetic aqueous rechargeable sodium-ion battery based on $Na_2CuFe(CN)_6$ - $NaTi_2(PO_4)_3$ intercalation chemistry.[J]. Chem Sus Chem, 2014, 7(2): 407−411

［18］ Chen L, Shao H, Zhou X, et al. Water-mediated cation intercalation of open-framework indium hexacyanoferrate with high voltage and fast kinetics[J]. Nature Communications, 2016, 7: 11982.1−11982.10

［19］ Li Z, Young D, Xiang K, et al. towards high power high energy aqueous sodium-ion batteries: the $NaTi_2(PO_4)_3$/$Na_{0.44}MnO_2$ system[J]. Advanced Energy Materials, 2013, 3(3): 290−294

［20］ Wu W, Shabhag S, Chang J, et al. Relating electrolyte concentration to performance and stability for $NaTi_2(PO_4)_3$/$Na_{0.44}MnO_2$ aqueous sodium-ion batteries[J]. Journal of the Electrochemical Society, 2015, 162(6): A803−A808

［21］ Whitacre J F, Tevar A, Sharma S. $Na_4Mn_9O_{18}$ as a positive electrode material for an aqueous electrolyte sodium-ion energy storage device[J]. Electrochemistry Communications, 2010, 12(3): 463−466

［22］ Wei C, Yu L, Cui C, et al. Ultrathin MnO_2 nanoflakes as efficient catalysts for oxygen reduction reaction[J]. Chemical Communications, 2014, 50(58): 7885−7888

［23］ Akimoto J, Hayakawa H, Kijima N, et al. Single-crystal synthesis and structure refinement of $Na_{0.44}MnO_2$. 17th International Conference on Solid Compounds of Transition Elements. Trans Tech Publications, 2011, 170: 198−202

［24］ Sauvage F, Laffont L, Tarascon J M, et al. study of the insertion/deinsertion mechanism of sodium into $Na_{0.44}MnO_2$[J]. Inorganic Chemistry, 2007, 46(8): 3289−3294

［25］ Ma G, Zhao Y, Huang K, et al. Effects of the starting materials of $Na_{0.44}MnO_2$ cathode materials on their electrochemical properties for Na-ion batteries[J]. Electrochim Acta, 2016, 222: 36−43

［26］ Cao Y, Xiao L, Wang W, et al. Reversible sodium ion insertion in single crystalline manganese oxide nanowires with long cycle life[J]. Advanced Materials, 2011, 23(28): 3155−3160